Juno's multi-instruments observations during the flybys of auroral bright spots in Jupiter's polar aurorae

K. Haewsantati[1,2,3], B. Bonfond[1], S. Wannawichian[3,4], G. R. Gladstone[5], V. Hue[5], T. K. Greathouse[5], D. Grodent[1], Z. Yao[6,1], J.-C. Gérard[1], R. Guo[7,1], S. Elliott[8,9], B. H. Mauk[10], G. Clark[10], D. Gershman[11], S. Kotsiaros[12,11], W. S. Kurth[8], J. Connerney[11], J. R. Szalay[13], A. Phriksee[3]

[1]LPAP, STAR Institute, Université de Liège, Liège, Belgium
[2]Ph.D. program in Physics, Department of Physics and Materials Science, Faculty of Science, Chiang Mai University, Chiang Mai, Thailand
[3]National Astronomical Research Institute of Thailand (Public Organization), Chiang Mai, Thailand
[4]Department of Physics and Materials Science, Faculty of Science, Chiang Mai University, Chiang Mai, Thailand
[5]Southwest Research Institute, San Antonio, Texas, USA
[6]Key Laboratory of Earth and Planetary Physics, Institute of Geology and Geophysics, Chinese Academy of Sciences, Beijing, China
[7]Laboratory of Optical Astronomy and Solar-Terrestrial Environment, Institute of Space Sciences, School of Space Science and Physics, Shandong University, Weihai, Shandong, China
[8]Department of Physics and Astronomy, University of Iowa, Iowa City, IA, USA
[9]School of Physics and Astronomy, University of Minnesota, Minneapolis, MN, USA
[10]The Johns Hopkins University Applied Physics Laboratory, Laurel, MD, USA
[11]NASA Goddard Space Flight Center, Greenbelt, MD, USA
[12]University of Maryland College Park, College Park, MD, USA
[13]Department of Astrophysical Sciences, Princeton University, Princeton, NJ, USA

Key Points:

- Jupiter's auroral bright spot emissions observed by Juno-UVS were simultaneously measured with the JADE, JEDI, Waves, and MAG instruments
- For each event, we observe characteristic changes of particle distributions and wave emissions, as well as magnetic field disturbances
- Whistler waves and electric currents appear to both play a role in the generation of bright auroral polar spots

Corresponding author: K. Haewsantati, K.Haewsantati@uliege.be

Abstract

Juno's arrival at Jupiter in 2016 revealed unprecedented details about Jupiter's ultraviolet aurorae thanks to its unique suite of remote sensing and in situ instruments. Here we present results from in situ observations during Juno flybys above specific bright auroral spots in Jupiter's polar aurora. We compare data observed by Juno-UVS, JEDI, JADE, Waves, and MAG instruments when Juno was magnetically connected to bright polar auroral spots during perijove 3 (PJ3), PJ15, and PJ33. The highly energetic particles observed by JEDI show enhancements dominated by upward electrons, which suggests that the particle acceleration region takes place below the spacecraft. Moreover, both brightness and upward particle flux were higher for the northern bright spot in PJ3 compared to the southern spots found in PJ15 and PJ33. In addition, we notice the intensification of whistler-mode waves at the time of the particle enhancements, suggesting that wave-particle interactions contribute to the acceleration of particles which cause the UV aurorae. The MAG data reveal magnetic perturbations during the PJ3 spot detection by Juno, which suggests the presence of significant field-aligned electric currents. While the stable position of the bright spots in System III suggests that the phenomenon is fixed with respect to the rotation of the planet, the presence of field-aligned currents leaves open the possibility of an origin rooted much farther in the magnetosphere.

1 Introduction

Jupiter's ultraviolet (UV) aurorae, the brightest of the solar system, are caused by high-energy particles precipitating along magnetic field lines and interacting with the neutral particles in Jupiter's upper atmosphere. The Jovian aurorae are usually divided into four components: the main emissions, the equatorward emissions, the polar emissions, and the satellite footprints. Each component exhibits different behaviors and morphologies depending on the specific processes from which they originate. In a previous work, we studied a feature in the polar aurora which we named a bright auroral spot (Haewsantati et al., 2021). This feature appears as a compact shape with a power on the order of ten GW. We found that the bright spots usually take the form of a quasi-periodic pulsation fixed in System III longitude position during the sequence. The spots are mostly located near the edge of the swirl region (Grodent et al., 2003), within the polar emissions. We suggested the source possibly corotates with Jupiter according to their fixed positions The bright spots are seen at all local times, which is not consistent with the idea of the simple Earth-like cusp process (Pallier & Prangé, 2001), which would be always oriented toward noon. However, Zhang et al. (2021) point out that the topology of Jupiter's magnetospheric cusp could be very complex. Therefore, we cannot totally exclude that the bright spot could be related to some cusp-like processes taking places in a complex and twisted polar magnetosphere.

The Juno spacecraft carries a comprehensive suite of instruments dedicated to Jupiter's magnetosphere and auroras (Bagenal et al., 2017). Juno moves along a very elliptical polar orbit and the close-up sequences, flying over Jupiter's pole from North to South, are typically named after their perijove (PJ) number. The morphology and spectral characteristics of the UV-aurorae are measured by the Ultraviolet Spectrograph (UVS) (Gladstone et al., 2017). UVS usually operates for several hours about each perijove, during which Juno is magnetically connected to numerous parts of the Jovian magnetosphere as the planet rotates beneath it. The auroras can also be observed remotely in the near-infrared by the Jupiter InfraRed Auroral Mapper (JIRAM) (Adriani et al., 2017). Juno in situ instruments provide critical insight on the magnetospheric processes leading to the Jovian aurorae. The plasma and energetic particles populations are measured with two instruments, the Jovian Auroral Distributions Experiment (JADE) (McComas et al., 2017) for the low energy particles and the Jupiter Energetic-particle Detector Instrument (JEDI) (Mauk, Haggerty, Jaskulek, et al., 2017) for the high energy particles. The character-

istics of electro-magnetic waves and magnetic field are observed by the Waves and MAG instruments, respectively (Connerney et al., 2017; Kurth et al., 2017).

A series of multi-instrument studies of auroral processes have been carried out over the last few years. Several studies directly compared in situ particle measurements with UVS observations, for example, Gérard et al. (2019), Allegrini, Mauk, et al. (2020), Ebert et al. (2019), and Szalay et al. (2020). The comparisons have been made between precipitating electron flux measured by JEDI and the auroral intensity observed by UVS by (Gérard et al., 2019). The results showed that the brightness of the main auroral emissions agree well with the brightness computed from JEDI electron energy flux. The brightness inferred from the JEDI measurements is computed using a model-derived rule-of-thumb that 1 mW/m^2 electron energy flux produces about 10 kilo-Rayleighs (kR) of total unabsorbed FUV H_2 emission. However, in the polar region, not only the observed upward particle energy flux is larger than the downward flux (Mauk, Haggerty, Paranicas, et al., 2017), but also the downward flux is not sufficient to produce the auroral UV emissions. Furthermore, the simultaneous observations of electron energy distributions from JADE and JEDI and the UV aurorae from UVS in the polar region during PJ5 (Ebert et al., 2019) showed that upward electron energy fluxes are greater than downward electron fluxes, the former being consistent with the UV emission recorded by UVS. Jupiter's auroras in the polar region have been found by Juno to be much more complex than anticipated. From plasma measurement by JADE, Szalay et al. (2017) presented five distinct regions associated with Jupiter's polar regions. Subsequently, the polar particle environment has been characterized into multiple zones corresponding to the character of pitch angle distributions and to the upward vs. downward flux (Mauk et al., 2020; Allegrini, Mauk, et al., 2020). Additionally, JEDI detected intense upward electron beams at energies greater than 1 MeV and connected to the swirl region in the polar auroral region (Paranicas et al., 2018). Also, electron inverted-V and proton and ions inverted-V were found over the polar cap (Mauk, Haggerty, Paranicas, et al., 2017; Clark, Mauk, Haggerty, et al., 2017; Clark, Mauk, Paranicas, et al., 2017; Mauk, Haggerty, Jaskulek, et al., 2017; Mauk et al., 2020). Intense upward whistler-mode waves have been observed by Waves above the polar region, which correlate with the detection of energetic electron precipitation by JEDI. The up-going electrons following an inverted-V pitch angle distribution are suggested to produce the upward whistler-mode waves (Elliott, Gurnett, Kurth, Mauk, et al., 2018; Elliott, Gurnett, Kurth, Clark, et al., 2018; Kurth et al., 2018; Elliott et al., 2020). Moreover, the interaction between these waves and particles could also play a role in the processes related to the auroral emissions.

We identified three unprecedented events during which Juno flew close to the field lines connecting to bright spot emissions. These occurrences took place during PJ3, PJ15, and PJ33 and we present here the results from in situ observations of the bright spot emissions made by UVS, Waves, JEDI, JADE, and MAG instruments. A short summary of each instrument is presented in Section 2. The observational results related to each event are presented in Section 3 and are discussed in Section 4.

2 Instruments and Observations

UVS is a photon-counting imaging ultraviolet spectrograph. The instrument is operated in the spectral range between 68 and 210 nm which covers the emissions in H_2 Lyman and Werner bands. A flat scan mirror at the entrance of the instrument can look at a target within $\pm$ 30° perpendicular to the spin plane. The "dog bone"-shaped slit consists of three contiguous segments with field of views of 0.2°$\times$ 2.5°, 0.025°$\times$ 2°, and 0.2°$\times$ 2.5°. Each photon, detected during every 30-sec spin of Juno, is attributed an X and Y position corresponding to the spectral dimension and spatial dimension, respectively (Gladstone et al., 2017; Greathouse et al., 2013; Hue et al., 2019). A spectral image of Jupiter's UV auroras is constructed based on the orientation of the scan mirror and the motion of the UVS field of view across the planet. A polar projection map is

created under the assumption that the auroras are emitted at an altitude of 400 km above the 1-bar pressure level (Bonfond et al., 2015). Since for each spin, near closest approach or perijove, the scan mirror generally points to different locations on Jupiter, a global view of the aurora may be reconstructed from several consecutive spins in each closest approach or each perijove (PJ). In this work we create a UV brightness map by combining spins in which we detected the bright auroral spot with 99 spins prior, which cover approximately 50 minutes time range (Bonfond et al., 2021). The brightness of the bright auroral spot is determined from the intensity of the last spin, in which the spot brightens. In our analysis, we convert the photon count rate to brightness in kR which, for the total unabsorbed H_2 Lyman emissions and Werner bands, may be obtained by multiplying the total counts obtained in the 155-162 nm wavelength range with the conversion factor of 8.1, based on an H_2 synthetic spectrum (Gustin et al., 2013). The brightness is then multiplied by the surface area and the mean energy of a UV photon to obtain the power emitted. The analysis method of the bright spot surface area is described in the previous study by Haewsantati et al. (2021). Since the brightness is integrated over a relatively large auroral region, the uncertainty due to the shot noise for a spot around 20 GW is of a few percent and can thus be neglected (Gérard et al., 2019). The main uncertainty on the auroral brightness determination is due to the in-flight calibration of the instrument's effective area (Hue et al., 2019). The FUV color ratio presented in this study is calculated by the ratio between the emission intensities of hydrogen molecule at wavelength range unaffected and affected by methane absorption, I (155–162 nm)/I (125–130 nm).

Juno's Waves instrument measures the electric field spectra from 50 Hz to 41 MHz and the magnetic field spectra from 50 Hz to 20 kHz. The instrument consists of a dipole electric antenna which is located perpendicular to the spacecraft's spin axis and x-axis and a 15-cm long magnetic search coil sensor whose axis is oriented parallel to the spacecraft's spin (z-axis) (Kurth et al., 2017). In this study, we use the Waves data with a sample rate of one spectrum per 1s. However, due to the limitations of single-axis measurement of electric and magnetic field, the wave properties cannot be completely analyzed. To determine whether they are electromagnetic or quasi-electrostatic, the wave mode can be identified by the electric to magnetic field ratio (E/cB), where c is the speed of light, along with characteristic frequencies of the plasma, such as the electron cyclotron frequency (F_{ce}) and the electron plasma frequency (F_{pe}), when detectable. A component of the direction of the Poynting flux can be determined by comparing the phase between the electric and magnetic signals under certain circumstances (Kolmašová et al., 2018). For further analysis, the cyclotron frequencies can be calculated with in situ measurements from the Magnetic Field Investigation (MAG) instrument (Connerney et al., 2017).

The JEDI instrument is a particle detector which measures the energy, angular, and compositional distributions of electrons (~ 25 to $\sim 1,200$ keV) and ions (~ 10 keV to >1.5 MeV for protons and ~ 150 keV to >100 MeV for oxygen and sulfur). The instrument consists of three sensors where two sensors (JEDI-90 and JEDI-270) are mounted on the spacecraft deck with the field of view covering $\sim 360^\circ$ along the plane roughly perpendicular to the Juno spin axis. JEDI-180 is oriented to cover nearly $\sim 180^\circ$ along Juno spin axis. Each sensor is comprised of a collimator, a time-of-flight (TOF) chamber, and a solid state detector (SSD) energy system (Mauk, Haggerty, Jaskulek, et al., 2017). The pitch angles can be calculated using the magnetic vector provided by the magnetometer on board Juno (Connerney et al., 2017). Details for caveats related to JEDI data are discussed in the supporting information of Mauk et al. (2018).

We can observe particles whose energies are lower than JEDI's energy range by using the Jovian Auroral Distribution Experiment or JADE (McComas et al., 2017). The instrument consists of two subsystems, JADE-E for electron measurements and JADE-I for ion measurements. The JADE-E measures electrons with 0.1-100 keV range. There are two identical sensors in use, which each have 120° field of view, to instantaneously

cover a total of 240° field of view in the azimuthal direction (perpendicular to the spin axis).

The Juno magnetometer (MAG) instrument consists of the Fluxgate Magnetometer (FGM) and Advanced Stellar Compass (ASC) CCD imagers. The three components of the magnetic field vectors in the range of ∼1 nT to ∼ 16x10^5 nT are measured by a pair of FGMs, together with the attitude determination system of the ASC. The MAG can observe each magnetic field component with a sample rate of 64, 32, or 16 measurements per second, depending on the distance between Juno and Jupiter. More details on the instruments are discussed in Connerney et al. (2017). Here we focus on the 1-s resolution magnetic field perturbations in each component during our focus time intervals. The perturbation is calculated by removing the estimated background field based on the Juno Reference Model through perijove 9 (JRM09) (Connerney et al., 2018) and the magnetodisc model (Connerney et al., 2020).

3 Results

3.1 PJ3 event

Figure 1 shows 100-spin maps of the UVS brightness and color ratio of the bright spot emission found during PJ3 on 11 Dec 2016: the last spin, which contain the bright spot, was acquired at 15:38:26 UT. The orange line represents the Juno footprint path according to the JRM09 model. It should be noted that there are some uncertainties on the mapping. For example, Allegrini, Gladstone, et al. (2020) reported a time delay of 90 s between the expected crossing time inferred from the UV brightness and JRM09 on one hand and the peak in the JADE electron flux on the other hand. At this time, the bright spot was located at latitude 64.3° N and 159.6° System III (SIII) longitude, with emitted power of ∼ 20 GW. This emission is found to be part of a bright spot emission sequence in which two emission peaks were detected before 15:21 UT and after 15:42 UT (with power 23 and 81 GW, respectively). This temporal sequence is presented in Haewsantati et al. (2021). However, there is a data gap, since the UVS scan mirror position was pointed at other auroral regions between 15:33 UT and 15:38 UT. Moreover, there are no clear bright spot data for approximately 4 mins after 15:38 UT until 15:42 UT, because of gaps in the UVS data stream and because the bright spot was in the area covered by the narrow slit. Even though the emission at 15:38 UT is not the peak emission in the sequence, this spot is considered because of the mapped positional proximity with Juno's magnetic footprint path.

Regarding the Waves observations, an intensification of whistler-mode hiss waves was observed from 15:36:30 UT until after 15:40:00 UT, as shown in top panel in Figure 2 (a zoom version of the wave plots are available in supporting information Figure S1). This intensification started a few seconds before the enhancement of upward electrons (second panel). The E/cB ratio analysis (see supporting information, Figure S2) shows that the waves are electromagnetic waves, indicated by the common value of electromagnetic whistler mode waves E/cB ratio between 1.0 and 2.0. Moreover, the Poynting flux analysis shows that, during the intensifications, a component of the Poynting flux direction is parallel to the magnetic field direction, implying that the waves propagate in the upward direction away from Jupiter for the northern hemisphere.

For JEDI data, we focus on the energy and pitch angle distributions of electrons as shown in Figure 2. The electron intensities started to increase at 15:37:47 UT, coinciding with the enhancement of the electric field spectral density (Figure 2a) until ∼15:42 UT. The time interval between 15:37 UT to 15:42 UT covers the time when the Juno spacecraft magnetic footprint passed closest to the bright spot position. The quantitative measure can be seen from the energy flux (Figure 2f). It should be noted that the magnetic mapping uncertainty prevents us from knowing the exact location of Juno's

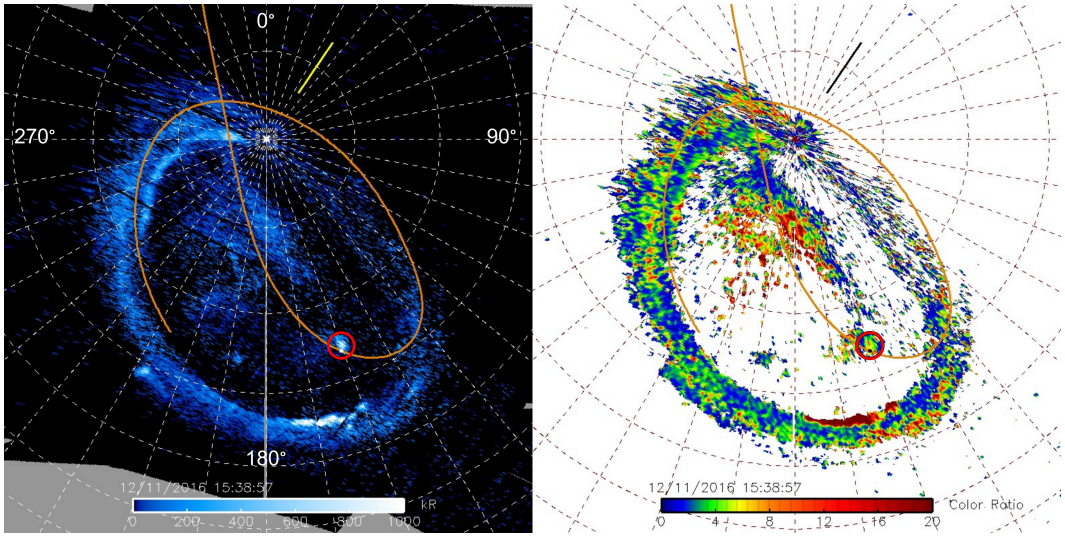

Figure 1. Polar projection showing a bright spot emission (red circle) in Jupiter's polar auroras as observed by UVS (left panel). The time presented here is the time of last spin where the bright auroral spot is detected. The grid consists of 10°spaced planetocentric parallels and SIII meridians. The right panel presents the color ratio, used as a proxy for the depth of the auroral emission.

footprint relative to the bright spot. However, we believe that Juno flew close enough that we can see the connection between the particle flux intensification and the bright spot appearance. The particle distributions are dominated by upward electrons throughout the interval of interest. During the time that Juno flew close to the bright spot position, i.e., at around 15:38 - 15:39 UT, the upward electron flux reached ~ 900 mW/m^2 while the energy flux of downward electrons was <70 mW/m^2. There are no appreciable fluxes of lower energy plasma observed by JADE, where only signatures of penetrating radiation are observed. As JEDI is able to measure the high energy charged particle environment, we focus on JEDI measurements for the remainder of this study.

Additionally, we studied the magnetic field perturbation at the time of the bright spot detection. The magnetic field perturbation (Figure 3) shows that, for PJ3, there was a deflection in all three components at $\sim$ 15:40 UT. These fluctuations, on the order of 100 nT, are significant and indicate the presence of strong field aligned currents (see Kotsiaros et al. (2019) for other examples).

3.2 PJ15 event

For the second identified event, a bright spot was found during PJ15, for the spin centered on 02:28:55 UT on 7 Sep 2018. In Figure 4, the bright spot position is 82.4° S and 58.2° SIII with emitted power of $\sim$ 6 GW, previously presented in Haewsantati et al. (2021) and characterized by a high color ratio (around 15), indicating high-energy particles precipitating into the atmosphere. The electric field spectral density observed by the Waves instrument (Figure 5a) also shows the intensifications of whistler-mode waves similar to those observed during PJ3. The E/cB ratio (see supporting information) and the Poynting flux analysis imply that the detected waves are electromagnetic and antiparallel to the magnetic field direction, indicating that waves were travelling upward away from Jupiter's southern hemisphere. The waves intensified before 02:28 UT and were damped

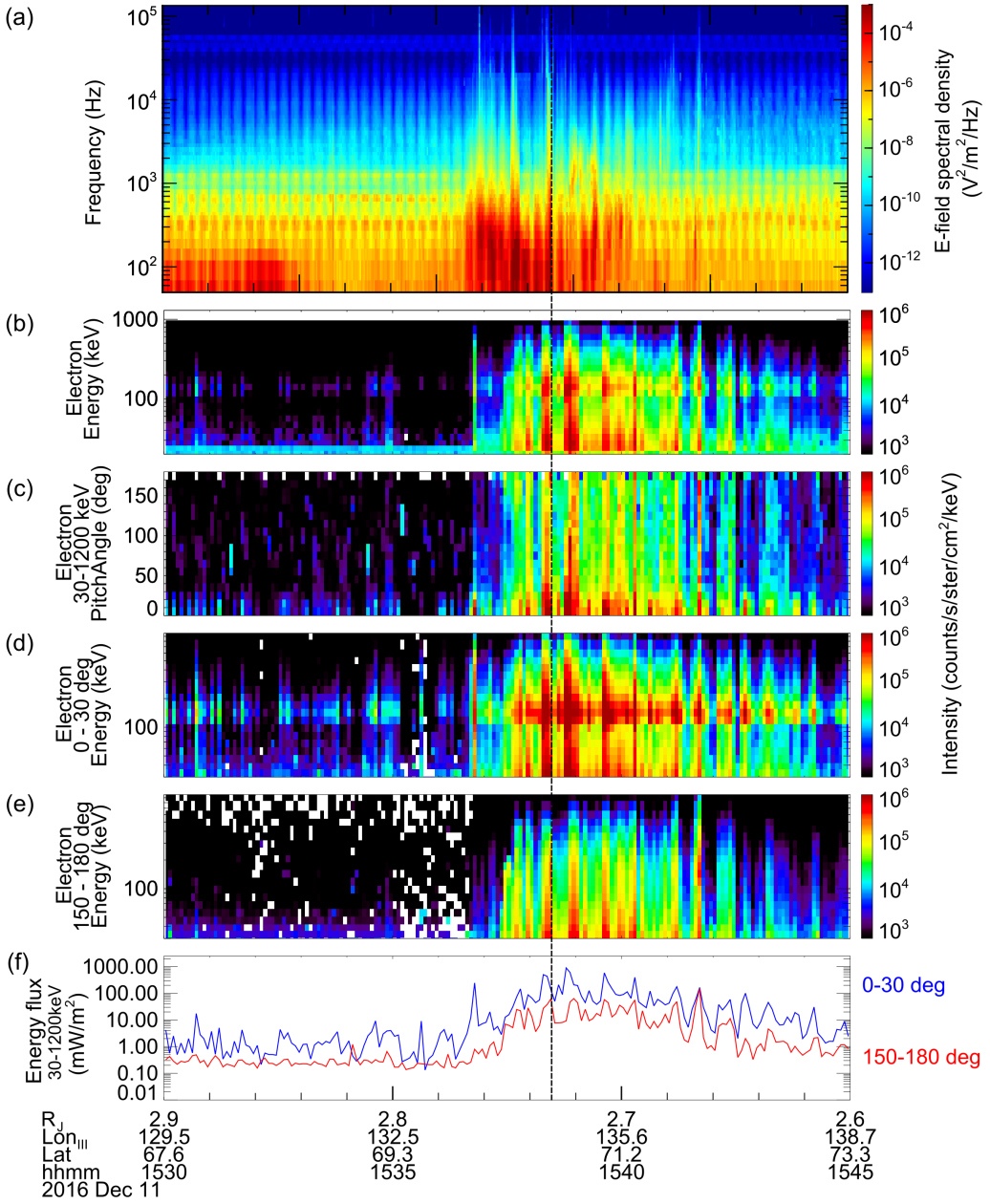

Figure 2. Observations of electric field spectral density and 5-s bin of electron energy distributions observed during PJ3: (a) the electric field spectral density observed by the Waves instrument, (b) total electron energy distributions, (c) pitch angle distributions, (d) energy distributions for upward electrons (pitch angles 0-30 °), (e) energy distributions for downward electrons (pitch angles 150-180 °), and (f) energy fluxes for upward (0-30 deg, blue line) and downward (150-180 deg, red line) electrons in the 30-1200 keV energy range. The vertical dashed line indicates the time of the bright spot crossing according to UVS and JRM09.

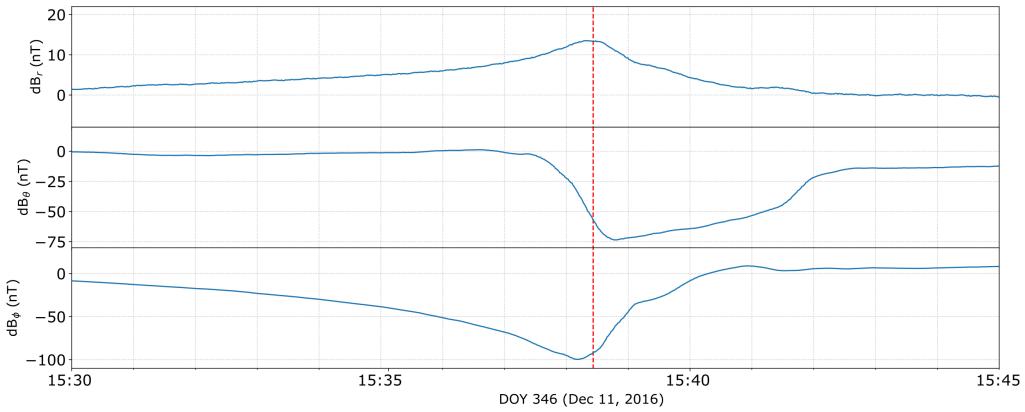

Figure 3. Magnetic field perturbation observed by Juno MAG during PJ3 showing the magnetic perturbation in each component. The time of bright spot detected by UVS indicated by red vertical line.

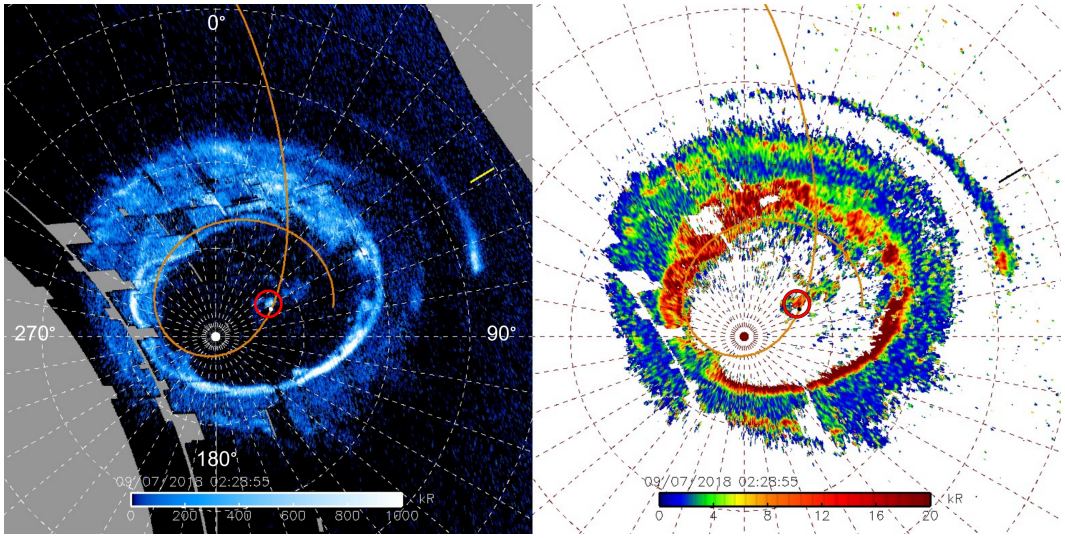

Figure 4. The polar projections with the same coordinates as Figure 1 shows bright spot emission and the color ratio distribution in Jupiter's polar auroras as observed by UVS from 100-spin where the last spin was when the magnetic footprint of Juno was close to the bright spot during PJ15 on 7 Sep 2018.

in the 02:28 - 02:30 UT range, which corresponds to the bright spot crossing according to the JRM09 magnetic field model.

As far as the pitch angle distribution is concerned, the JEDI energy flux in Figure 5 shows the same trend as found in PJ3, in which the upward electrons are dominating during the time interval of interest. However, the energy distribution shows only small fluctuations, with 1) an intensification dominated by upward electrons just before 02:25 UT, i.e. right before Waves observed its intensification and 2) two intensifications near 02:30 UT. The last two panels near 02:30 UT clearly show that the enhancements are from upward electrons. Note that the bright spot was observed at ∼02:29 UT. The upward electrons energy flux of two peaks is 30-40 mW/m^2, while the energy flux of downward electrons is <5 mW/m^2. These energy fluxes of 30-40 mW/m^2 are lower than dur-

ing the PJ3 event, in agreement with the lower emitted power recorded by UVS. A magnetic field deflection associated with that event was recorded in all three components (Figure 6), but its amplitude is quite limited (∼20 nT). In summary, the in situ signatures of the crossing are less prominent than for the PJ3 case, partly because of the lower emitted power recorded by UVS, combined with the uncertainty in the magnetic mapping which may have caused the crossing to take place farther from the peak.

3.3 PJ33 event

The third event is a southern bright spot found during PJ33, as shown in Figure 7. The bright spot was seen at 01:38:30 UT on 16 Apr 2021 with a power of ∼10 GW at 83.5° S and 59.5° SIII. No significant deflection of the magnetic field could be measured by the MAG instrument (Figure 9) at the time of the waves intensifications and electron enhancements during PJ33. The electric field spectral density plot from Waves observations (Figure 8a) shows some intensifications above the proton cyclotron frequency, which is the whistler-mode wave, at ∼ 01:33-01:37 UT. However, there are no burst waveforms for the Poynting flux analysis. Therefore, the direction of the Poynting flux cannot be determined during this time interval.

Moreover, the intensity enhancement was found at ∼01:33 UT – 01:35 UT, as shown in the JEDI plots (Figure 8). The enhancement is clearly seen in the upward polar electron beam data whose energy is higher than 500 keV. Upward electrons were previously observed over the polar auroral region, though at intensities more modest (Mauk et al., 2020). JEDI measured an enhancement in the proton flux at ∼01:35 UT. Protons were first moving downward and then the low energy protons with perpendicular pitch angle became more dominant. However, the electron energy flux decreased after 01:35 UT and continued to be small during the UVS bright spot detection time (01:38 UT). Then two peaks in the particle flux appear around 01:46 UT. It is noteworthy that the time of the most intense bright spot emissions does not exactly correspond to the time of the most intense upward particle flux. This suggest that Juno did not cross the field line connected to the bright spot when the UV emitted power is maximum. As shown in Table 1, the altitude of Juno during PJ33 was even higher than during PJ3 and PJ15. It appears that the processes accelerating particle either downward to the aurora or upward to the magnetosphere took place below the spacecraft.

4 Discussions and Conclusions

We present in situ and UV imaging observations during the time of the brightening of bright spot emissions. The summary and comparison of the data from all instruments are shown in Table 1. The crossing time duration is on the order of 3-4 minutes for PJ3 and PJ15 and 12 minutes for PJ33. On the other hand, the brightness variation time interval of the emission bright spot, ∼5 minutes. (Haewsantati et al., 2021), is comparable to the crossing time. We have to take this timing information into account when interpreting the data set. Based on the UVS data, the PJ3 emitted power is 2-3 times more energetic than the PJ15 and PJ33 events. No discernable plasma signatures were observed below 50 keV in JADE, where only signatures of penetrating radiation were observed. Moreover, an enhancement of upward electron flux observed by JEDI are found in all three events. In all three cases, the bright spot, which is the signature of an intense flux of down-going particles, corresponds to the enhanced electron fluxes in the upward direction as well. We note that both the energy flux and the bright spot power for PJ3 are relatively high compared to the other two cases. The dominance of upward electrons combined with intense auroral emissions suggests that most of the electron acceleration takes place between the spacecraft and the planet, in both directions along the field lines.

It is interesting to note that the magnetic perturbations in PJ15 and PJ33 do not show strong signatures as found in PJ3. Therefore, the magnetospheric currents might

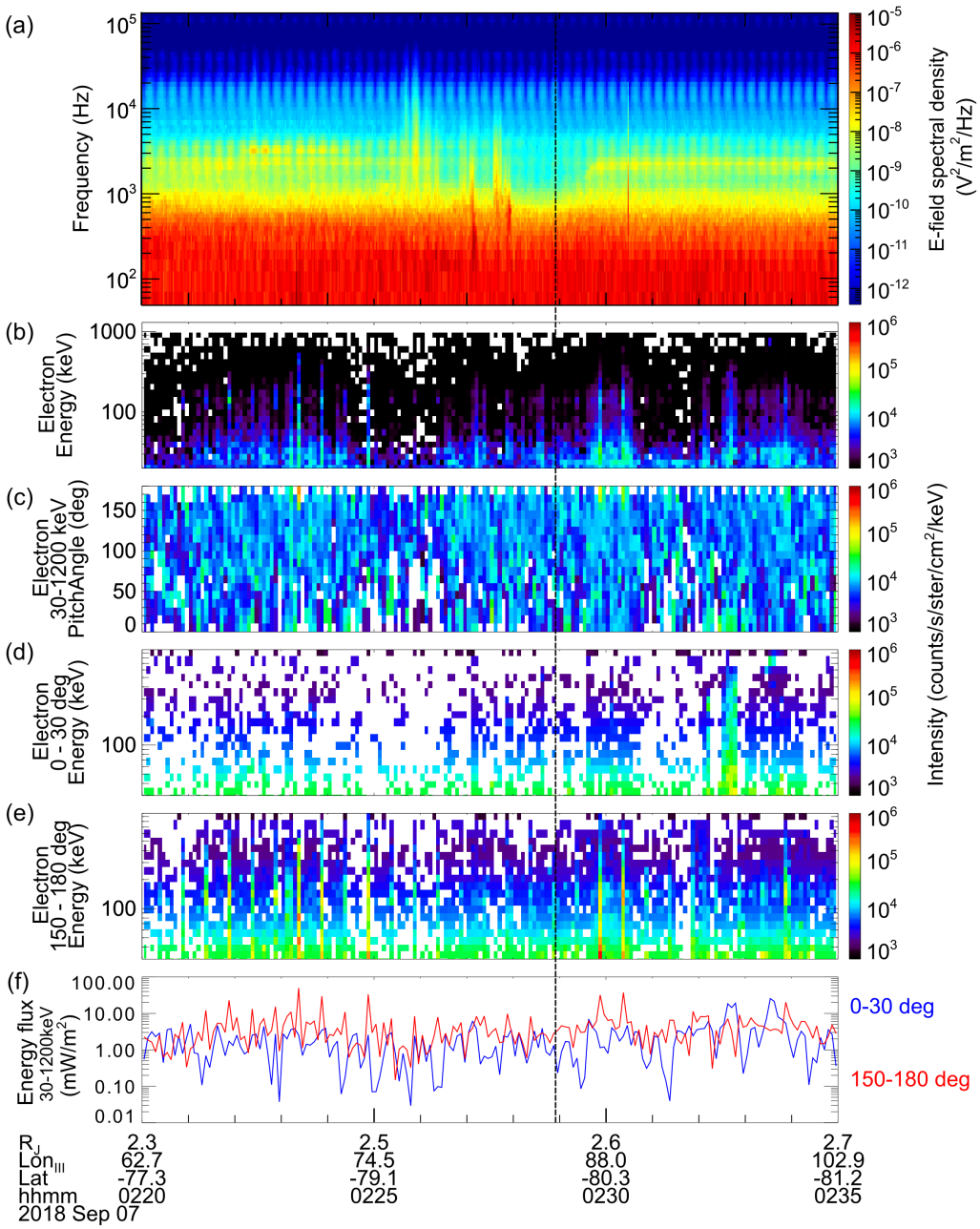

Figure 5. Observations of electric field spectral density and 5-s bin of electron energy distributions observed during PJ15, each panel is the same observation as described in Figure 2. For southern hemisphere, electrons with pitch angles 150-180 °and 0-30 °are upward and downward electrons, respectively. The energy fluxes (f) of upward electrons are presented by red line and blue line for downward electrons.

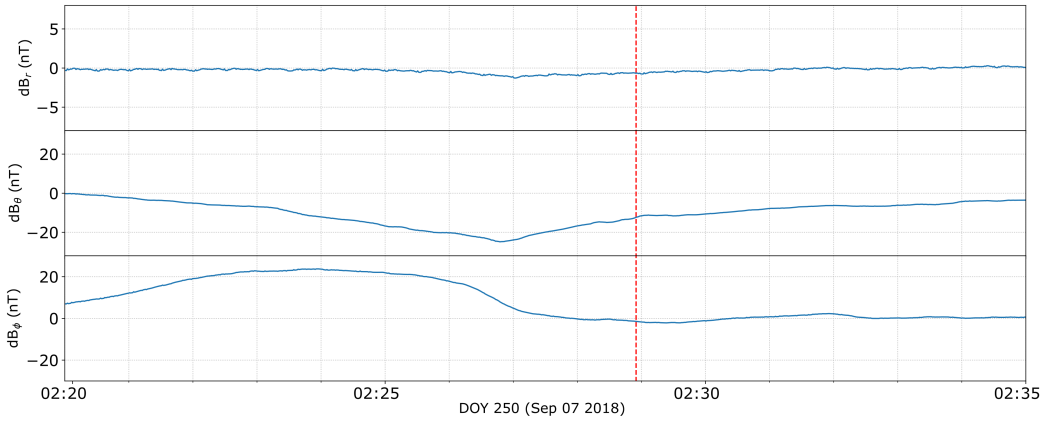

Figure 6. Magnetic field perturbation observed by Juno MAG during PJ15 showing the magnetic perturbation in each component. The time of bright spot detected by UVS indicated by red vertical line.

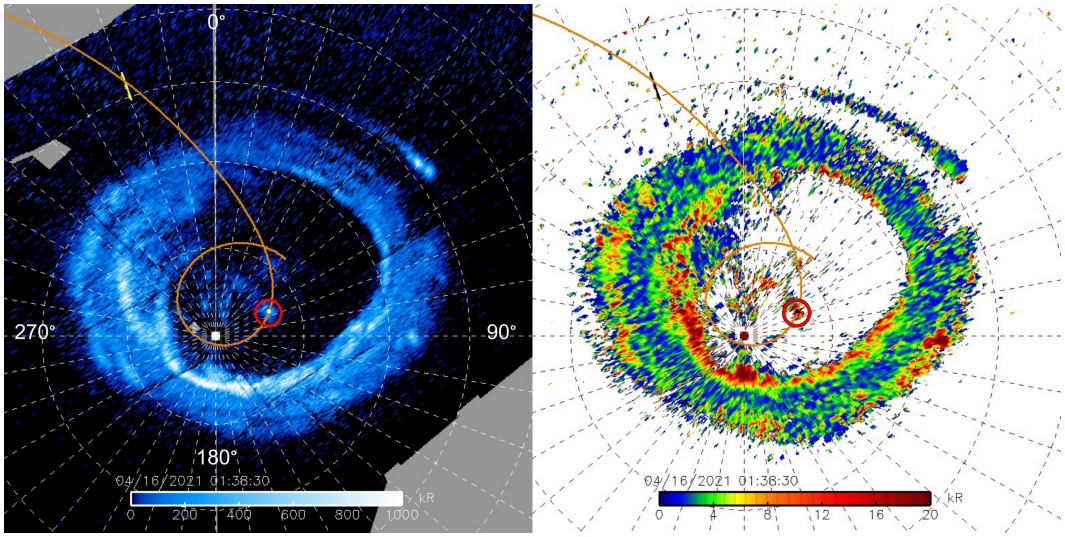

Figure 7. When the spacecraft flew closed to the bright spot position during PJ33 on 16 Apr 2021, the polar projection shows bright spot emission in Jupiter's polar auroras (left) and color ratio (right) as observed by UVS combined from 100-spin, with the last spin centered on 01:38:30 UT. The coordinates are same as described in Figure 1.

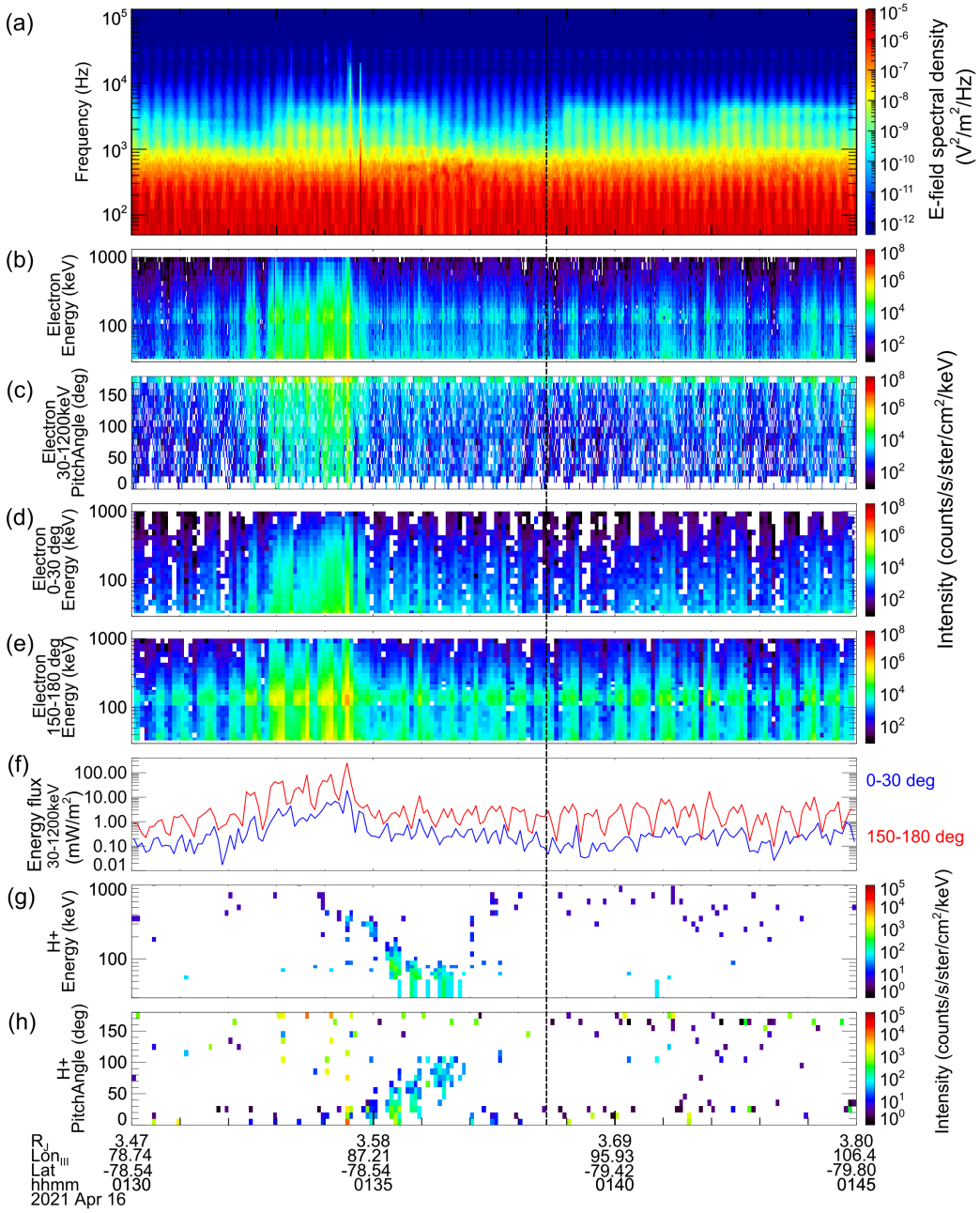

Figure 8. Observations of electric field spectral density by Waves and particle distributions made by JEDI instrument during PJ33. Panel (a) to (f) are similar description as Figure 2 and particle directions are similar as describe in 5.The proton energy distributions and pitch angle distributions are shown in panel (g) and (h), respectively.

Table 1. Summary data for bright spot in situ observation

		PJ3	PJ15	PJ33
Date		11-Dec-16	7-Sep-18	16-Apr-21
Juno footprint position (Lat, SIII Lon)		(63.65°, 160.20°)	(-83.04°,63.93°)	(-83.37°,65.50°)
Juno altitude (R_J)		1.8-1.7	1.5-1.6	2.58-2.69
Bright spot crossing time (UT)		15:38:26	02:28:55	01:38:30
Bright spot position (Lat, SIII Lon)		(64.38°, 159.61°)	(-82.88°, 58.19°)	(-83.51°, 59.50°)
Bright spot power (GW)		15.30	5.58	10.81
JEDI	**electron direction and enhancement time**	Upward during 15:36 UT - 15:42 UT	Upward, 2 peaks (31.9 and 37.4 at time ∼ 02:30 UT)	Upward during 01:33 UT - 01:35 UT
	maximum electron energy flux (mW/m^2)	899.82 at 15:38:47 UT	49.62 at 02:23:22 UT	860.52 at 01:34:29 UT
	electron direction[a]	Upward	Upward	Upward
	average electron energy flux[b] **(mW/m^2)**	267.24	3.1	0.22
	proton direction	upward	upward	upward then perpendicular
Waves	**Whistler-mode intensification**	15:37 UT - 15:40 UT	02:26 UT - 02:28 UT	01:33 UT - 01:37 UT
	waves direction	upgoing	upgoing	no analysis
MAG		A perturbation with small amplitude during 15:38 UT - 15:42 UT	A small deflection but less obvious	no significant deflection

[a]at bright spot crossing time
[b]during bright spot crossing (±10 s)

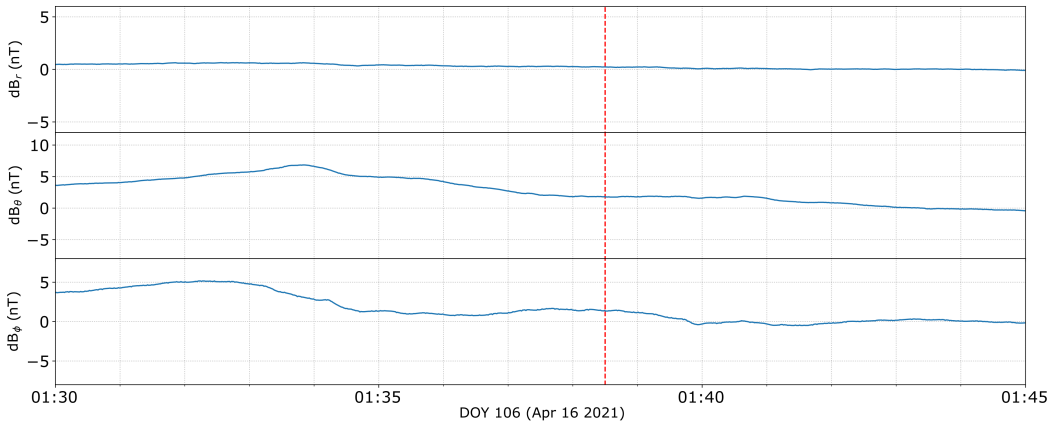

Figure 9. Magnetic field perturbation observed by Juno MAG during PJ33 showing the magnetic perturbation in each component. The time of bright spot detected by UVS indicated by red vertical line.

not play a major role on bright spot emission. However, the strong deflection detected during PJ3 is most probably a signature of significant field-aligned currents on (or very near) the flux tubes crossed by Juno.

Regarding the wave-particle interactions, the upgoing whistler-mode waves are related to the upward energetic electron beams in the Jovian polar cap (Elliott et al., 2020). Moreover, the upgoing electrons were suggested to be stochastically accelerated by the broadband whistler mode waves (Elliott, Gurnett, Kurth, Mauk, et al., 2018; Elliott et al., 2020). The concurrent intensification of JEDI and Waves data in PJ3, PJ15, and PJ33 strongly support these arguments. We notice that whistler-mode waves occurred a few seconds before the detection of an upward electron enhancement during PJ3. This enhancement started when Juno flew close to the bright spot position. In addition, the intensification of whistler-mode waves happened nearly at the same time with electron enhancement in PJ33 event. For PJ15, we also found that, where the altitude increases with time, the whistler-mode waves were first enhanced and then damped for ~ 2 minutes during the bright spot crossing but just before the electron enhancement. This behavior suggests that energy transfer between waves and particles is taking place, as discussed in Elliott, Gurnett, Kurth, Mauk, et al. (2018). According to this theory, waves are generated close to the planet (i.e. at smaller radial distances) and then propagate along the magnetic field lines toward higher altitudes to become damped, transferring their energy to the electrons, which can then be accelerated. Since the bright spots were detected during the same time of the wave damping and following by electron enhancements, we suggest that these waves contribute to the acceleration of particles that cause the UV emissions.

Figure 10 shows the Juno-UVS measurement of noise count rates during the Juno bright spot flyby. The noise count rates here are due to >7 MeV electrons penetrating the instrument's shielding (Zhu et al., 2021). The blue vertical lines in the plots represent the times when UVS's line of sight is aligned with the magnetic field (points away from Jupiter for PJ3 and toward Jupiter for PJ15 and PJ33). The red line presents the Juno altitude during the polar crossing. For PJ15 and PJ33, the count rates reach a peak value when UVS points toward Jupiter as shown by the bar code patterns (Bonfond et al., 2018). For PJ3, the count rate peaks are in between the blue lines, the data gaps do not allow for a clear identification of the orientation of the penetrating electrons. On the other hand, on PJ15, the count rate is very low suggesting there were only typical back-

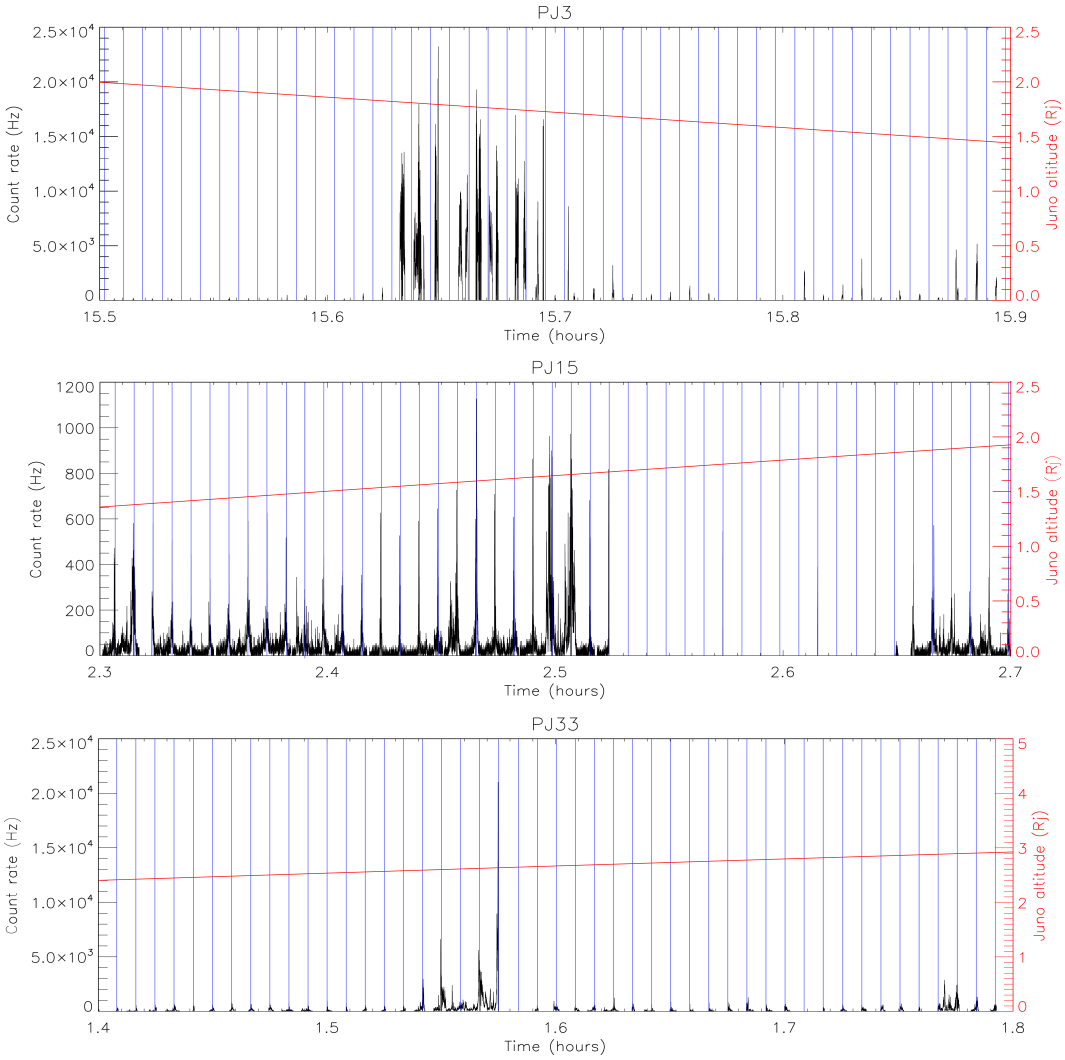

Figure 10. Penetrating particle count rate measured by Juno-UVS during (top) PJ3, (middle) PJ15, and (bottom) PJ33. The zero count rate refers the data gap. The times when Juno-UVS aligned with minimum angle to the magnetic field lines are shown by vertical blue lines. The evolution of Juno altitude is represented by the red line.

ground noise signals. Overall, the counts rates peak at the same time as the wave-particle enhancements for all three events. These contemporary results agree with the fact that we have a relative increase in flux of upgoing particles seen in both UVS and JEDI. One hypothesis is that we see the high energy tail of the particles related to the upward electron and upgoing whistler mode waves interaction as described by Elliott, Gurnett, Kurth, Mauk, et al. (2018).

It must be noted that there are the possible time delays between UVS observation and waves and particles observation, which could be the explanation for the time differences between wave and particle enhancements and bright spot detection. Several scenarios are proposed, as follows. Firstly, if we consider that Juno was crossing magnetic field lines mapped to the emission spot, the observation times of the waves and particles should be prior to the bright spot emission time, since waves and particles should take some time to travel from the spacecraft to the bright spot position beneath the space-

craft. To estimate how long the particles would take for travelling, the travel times of 100 keV electron and 100 keV proton for a distance ~ 1.5 R_J from the spacecraft to the bright spot position are 0.6 s and 25 s, respectively, while the wave traveling time is even shorter. As a result, the travel times of waves and particles should not be the cause of the time differences between UVS spots and wave-particle enhancement detections. As a comparison, the spin period of the spacecraft is 30 secs, which is longer than the travel time of even the protons. Secondly, the bright spot is evolving with time and the UVS image might capture it with a different brightness or with a different extent, in comparison to the time of field line crossing. This source of uncertainty would explain the mismatch in intensity rather than a time difference. Finally, the mapping from the JRM09 magnetic field model is not perfectly accurate and errors could translate into a time delay (i.e., Allegrini, Gladstone, et al. (2020)).

Overall, for the processes related to the bright spot emissions, intense field-aligned currents do not seem to be a necessary condition for bright spot emissions, as none were detected for PJ15 or PJ33. On the other hand, the fact that the bright spots are almost fixed in System III indicates that the processes giving rise to them are anchored to the planet. With supporting information from Waves (presence of whistler mode waves) and JEDI (up-ward electron beam), wave-particle interactions associated with whistler mode waves (Elliott, Gurnett, Kurth, Mauk, et al., 2018) appears as the most plausible process causing the particle acceleration leading to the auroral bright spot emission. However, two recent alternative scenarios should also be taken into consideration: 1) magnetic reconnection at Jupiter's near-planet polar magnetosphere, which could generate high-energy electron beams (Masters et al., 2021), and 2) the broadband acceleration due to the presence of an ionospheric Alfvén resonator or IAR (Lysak et al., 2021). In order to better identify the root cause for these intriguing bright spot emissions, further information could possibly be found by looking deeper into the high-resolution magnetohydrodynamic simulations of the Jovian magnetosphere and the tangling of the magnetic flux tubes above the poles (see, for example, Zhang et al. (2021)). Other promising investigations would result from the future flybys over the bright spot through or below the particle acceleration region, sampling the downgoing particles and providing a direct link between the particle's behaviors and the emissions.

Acknowledgments

The authors are grateful to NASA and contributing institutions which have made the Juno mission possible. We thank Masafumi Imai for providing the Juno footpath tracing. We also thank Marissa Vogt for providing the code to compute Jupiter's magnetic field based on JRM09 model (`https://github.com/marissav06/jovian_jrm09_internal`). K. Haewsantati would like to acknowledge for Science Achievement Scholarship of Thailand (SAST) and Ph.D. program in Physics, Chiang Mai University. K. Haewsantati and S. Wannawichian are financial supported by National Astronomical Research Institute of Thailand (NARIT). Additional support was from Thailand Science Research and Innovation grant RTA6280002. B. Bonfond is a Research Associate of the Fonds de la Recherche Scientifique - FNRS. B. Bonfond, D. Grodent, and J.-C. Gérard are funded by the Belgian Federal Science Policy Office (BELSPO) via the PRODEX Program of European Space Agency (ESA). Z. Yao was supported by the National Science Foundation of China (grant 42074211) and Key Research Program of the Institute of Geology & Geophysics CAS (grant IGGCAS-201904). J. R. Szalay was supported by Juno's NASA contract NNM06AA75C. The research at the University of Iowa is supported by NASA through Contract 699041X with Southwest Research Institute. UVS data used herein is found in the Planetary Data System (PDS) `https://pds.nasa.gov` at doi.org/10.17189/1518951. Waves survey data are at doi.org/10.17189/1520498. Juno Magnetometer data are at doi:10.17189/1519711. JEDI data are at doi:10.17189/1519713. JADE data may be found at doi:10.17189/1519715.

References

Adriani, A., Filacchione, G., Di Iorio, T., Turrini, D., Noschese, R., Cicchetti, A., ... Olivieri, A. (2017). JIRAM, the Jovian Infrared Auroral Mapper. *Space Science Reviews*, *213*(1), 393–446. doi: 10.1007/s11214-014-0094-y

Allegrini, F., Gladstone, G. R., Hue, V., Clark, G., Szalay, J. R., Kurth, W. S., ... Wilson, R. J. (2020). First Report of Electron Measurements During a Europa Footprint Tail Crossing by Juno. *Geophysical Research Letters*, *47*(18), e2020GL089732. (e2020GL089732 2020GL089732) doi: 10.1029/2020GL089732

Allegrini, F., Mauk, B., Clark, G., Gladstone, G. R., Hue, V., Kurth, W. S., ... Wilson, R. J. (2020). Energy Flux and Characteristic Energy of Electrons Over Jupiter's Main Auroral Emission. *Journal of Geophysical Research: Space Physics*, *125*(4), e2019JA027693. doi: 10.1029/2019JA027693

Bagenal, F., Adriani, A., Allegrini, F., Bolton, S. J., Bonfond, B., Bunce, E. J., ... Zarka, P. (2017). Magnetospheric Science Objectives of the Juno Mission. *Space Science Reviews*, *213*(1-4), 219–287. doi: 10.1007/s11214-014-0036-8

Bonfond, B., Gladstone, G. R., Grodent, D., Gérard, J.-C., Greathouse, T. K., Hue, V., ... Connerney, J. E. P. (2018). Bar Code Events in the Juno-UVS Data: Signature ∼10 MeV Electron Microbursts at Jupiter. *Geophysical Research Letters*, *45*(22), 12,108–12,115. doi: 10.1029/2018GL080490

Bonfond, B., Gustin, J., Gérard, J.-C., Grodent, D., Radioti, A., Palmaerts, B., ... Tao, C. (2015). The far-ultraviolet main auroral emission at Jupiter – Part 2: Vertical emission profile. *Annales Geophysicae*, *33*(10), 1211–1219. doi: 10.5194/angeo-33-1211-2015

Bonfond, B., Yao, Z. H., Gladstone, G. R., Grodent, D., Gérard, J.-C., Matar, J., ... Bolton, S. J. (2021). Are Dawn Storms Jupiter's Auroral Substorms? *AGU Advances*, *2*(1), e2020AV000275. (e2020AV000275 2020AV000275) doi: 10.1029/2020AV000275

Clark, G., Mauk, B. H., Haggerty, D., Paranicas, C., Kollmann, P., Rymer, A., ... Valek, P. (2017). Energetic particle signatures of magnetic field-aligned potentials over Jupiter's polar regions. *Geophysical Research Letters*, *44*(17), 8703–8711. doi: 10.1002/2017GL074366

Clark, G., Mauk, B. H., Paranicas, C., Haggerty, D., Kollmann, P., Rymer, A., ... Valek, P. (2017). Observation and interpretation of energetic ion conics in Jupiter's polar magnetosphere. *Geophysical Research Letters*, *44*(10), 4419–4425. doi: 10.1002/2016GL072325

Connerney, J. E. P., Benn, M., Bjarno, J. B., Denver, T., Espley, J., Jorgensen, J. L., ... Smith, E. J. (2017). The Juno Magnetic Field Investigation. *Space Science Reviews*, *213*(1), 39–138. doi: 10.1007/s11214-017-0334-z

Connerney, J. E. P., Kotsiaros, S., Oliversen, R. J., Espley, J. R., Joergensen, J. L., Joergensen, P. S., ... Levin, S. M. (2018). A New Model of Jupiter's Magnetic Field From Juno's First Nine Orbits. *Geophysical Research Letters*, *45*(6), 2590–2596. doi: 10.1002/2018GL077312

Connerney, J. E. P., Timmins, S., Herceg, M., & Joergensen, J. L. (2020). A Jovian Magnetodisc Model for the Juno Era. *Journal of Geophysical Research: Space Physics*, *125*(10), e2020JA028138. (e2020JA028138 2020JA028138) doi: 10.1029/2020JA028138

Ebert, R. W., Greathouse, T. K., Clark, G., Allegrini, F., Bagenal, F., Bolton, S. J., ... Wilson, R. J. (2019). Comparing Electron Energetics and UV Brightness in Jupiter's Northern Polar Region During Juno Perijove 5. *Geophysical Research Letters*, *46*(1), 19–27. doi: 10.1029/2018GL081129

Elliott, S. S., Gurnett, D. A., Kurth, W. S., Clark, G., Mauk, B. H., Bolton, S. J., ... Levin, S. M. (2018). Pitch Angle Scattering of Upgoing Electron Beams in Jupiter's Polar Regions by Whistler Mode Waves. *Geophysical Research Letters*, *45*(3), 1246–1252. doi: 10.1002/2017GL076878

Elliott, S. S., Gurnett, D. A., Kurth, W. S., Mauk, B. H., Ebert, R. W., Clark, G., ... Bolton, S. J. (2018). The Acceleration of Electrons to High Energies Over the Jovian Polar Cap via Whistler Mode Wave-Particle Interactions. *Journal of Geophysical Research: Space Physics*, *123*(9), 7523–7533. doi: 10.1029/2018JA025797

Elliott, S. S., Gurnett, D. A., Yoon, P. H., Kurth, W. S., Mauk, B. H., Ebert, R. W., ... Sulaiman, A. H. (2020). The Generation of Upward-Propagating Whistler Mode Waves by Electron Beams in the Jovian Polar Regions. *Journal of Geophysical Research: Space Physics*, *125*(6), e2020JA027868. doi: 10.1029/2020JA027868

Gérard, J.-C., Bonfond, B., Mauk, B. H., Gladstone, G. R., Yao, Z. H., Greathouse, T. K., ... Levin, S. M. (2019). Contemporaneous Observations of Jovian Energetic Auroral Electrons and Ultraviolet Emissions by the Juno Spacecraft. *Journal of Geophysical Research: Space Physics*, *124*(11), 8298–8317. doi: 10.1029/2019JA026862

Gladstone, G. R., Persyn, S. C., Eterno, J. S., Walther, B. C., Slater, D. C., Davis, M. W., ... Denis, F. (2017). The Ultraviolet Spectrograph on NASA's Juno Mission. *Space Science Reviews*, *213*(1-4), 447–473. doi: 10.1007/s11214-014-0040-z

Greathouse, T. K., Gladstone, G. R., Davis, M. W., Slater, D. C., Versteeg, M. H., Persson, K. B., ... Eterno, J. S. (2013). Performance results from in-flight commissioning of the Juno Ultraviolet Spectrograph (Juno-UVS). In *UV, X-Ray, and Gamma-Ray Space Instrumentation for Astronomy XVIII* (Vol. 8859, p. 88590T). International Society for Optics and Photonics. doi: 10.1117/12.2024537

Grodent, D., Clarke, J. T., Waite, J. H., Cowley, S. W. H., Gérard, J.-C., & Kim, J. (2003). Jupiter's polar auroral emissions. *Journal of Geophysical Research: Space Physics*, *108*(A10). doi: 10.1029/2003JA010017

Gustin, J., Gérard, J. C., Grodent, D., Gladstone, G. R., Clarke, J. T., Pryor, W. R., ... Ajello, J. M. (2013). Effects of methane on giant planet's UV emissions and implications for the auroral characteristics. *Journal of Molecular Spectroscopy*, *291*, 108–117. doi: 10.1016/j.jms.2013.03.010

Haewsantati, K., Bonfond, B., Wannawichian, S., Gladstone, G. R., Hue, V., Versteeg, M. H., ... Vogt, M. F. (2021). Morphology of Jupiter's Polar Auroral Bright Spot Emissions via Juno-UVS Observations. *Journal of Geophysical Research: Space Physics*, *126*(2), e2020JA028586. doi: 10.1029/2020JA028586

Hue, V., Gladstone, G. R., Greathouse, T. K., Kammer, J. A., Davis, M. W., Bonfond, B., ... Byron, B. D. (2019). In-flight Characterization and Calibration of the Juno-ultraviolet Spectrograph (Juno-UVS). *The Astronomical Journal*, *157*(2), 90. doi: 10.3847/1538-3881/aafb36

Kolmašová, I., Imai, M., Santolík, O., Kurth, W. S., Hospodarsky, G. B., Gurnett, D. A., ... Bolton, S. J. (2018). Discovery of rapid whistlers close to Jupiter implying lightning rates similar to those on Earth. *Nature Astronomy*, *2*(7), 544–548. doi: 10.1038/s41550-018-0442-z

Kotsiaros, S., Connerney, J. E. P., Clark, G., Allegrini, F., Gladstone, G. R., Kurth, W. S., ... Levin, S. M. (2019). Birkeland currents in Jupiter's magnetosphere observed by the polar-orbiting Juno spacecraft. *Nature Astronomy*, *3*(10), 904–909. doi: 10.1038/s41550-019-0819-7

Kurth, W. S., Hospodarsky, G. B., Kirchner, D. L., Mokrzycki, B. T., Averkamp, T. F., Robison, W. T., ... Zarka, P. (2017). The Juno Waves Investigation. *Space Science Reviews*, *213*(1), 347–392. doi: 10.1007/s11214-017-0396-y

Kurth, W. S., Mauk, B. H., Elliott, S. S., Gurnett, D. A., Hospodarsky, G. B., Santolik, O., ... Levin, S. M. (2018). Whistler Mode Waves Associated With Broadband Auroral Electron Precipitation at Jupiter. *Geophysical Research Letters*, *45*(18), 9372–9379. doi: 10.1029/2018GL078566

Lysak, R. L., Song, Y., Elliott, S., Kurth, W., Sulaiman, A. H., & Gershman, D. (2021). The jovian ionospheric alfvén resonator and auroral particle acceleration. *Journal of Geophysical Research: Space Physics*, *126*(12), e2021JA029886. Retrieved from `https://agupubs.onlinelibrary.wiley.com/doi/abs/10.1029/2021JA029886` (e2021JA029886 2021JA029886) doi: https://doi.org/10.1029/2021JA029886

Masters, A., Dunn, W. R., Stallard, T. S., Manners, H., & Stawarz, J. (2021). Magnetic Reconnection Near the Planet as a Possible Driver of Jupiter's Mysterious Polar Auroras. *Journal of Geophysical Research: Space Physics*, *126*(8), e2021JA029544. (e2021JA029544 2021JA029544) doi: 10.1029/2021JA029544

Mauk, B. H., Clark, G., Gladstone, G. R., Kotsiaros, S., Adriani, A., Allegrini, F., ... Rymer, A. M. (2020). Energetic Particles and Acceleration Regions Over Jupiter's Polar Cap and Main Aurora: A Broad Overview. *Journal of Geophysical Research: Space Physics*, *125*(3), e2019JA027699. doi: 10.1029/2019JA027699

Mauk, B. H., Haggerty, D. K., Jaskulek, S. E., Schlemm, C. E., Brown, L. E., Cooper, S. A., ... Stokes, M. R. (2017). The Jupiter Energetic Particle Detector Instrument (JEDI) Investigation for the Juno Mission. *Space Science Reviews*, *213*(1), 289–346. doi: 10.1007/s11214-013-0025-3

Mauk, B. H., Haggerty, D. K., Paranicas, C., Clark, G., Kollmann, P., Rymer, A. M., ... Valek, P. (2017). Juno observations of energetic charged particles over Jupiter's polar regions: Analysis of monodirectional and bidirectional electron beams. *Geophysical Research Letters*, *44*(10), 4410–4418. doi: 10.1002/2016GL072286

Mauk, B. H., Haggerty, D. K., Paranicas, C., Clark, G., Kollmann, P., Rymer, A. M., ... Valek, P. (2018). Diverse Electron and Ion Acceleration Characteristics Observed Over Jupiter's Main Aurora. *Geophysical Research Letters*, *45*(3), 1277–1285. doi: 10.1002/2017GL076901

McComas, D. J., Alexander, N., Allegrini, F., Bagenal, F., Beebe, C., Clark, G., ... White, D. (2017). The Jovian Auroral Distributions Experiment (JADE) on the Juno Mission to Jupiter. *Space Science Reviews*, *213*(1), 547–643. doi: 10.1007/s11214-013-9990-9

Pallier, L., & Prangé, R. (2001). More about the structure of the high latitude Jovian aurorae. *Planetary and Space Science*, *49*(10), 1159–1173. doi: 10.1016/S0032-0633(01)00023-X

Paranicas, C., Mauk, B. H., Haggerty, D. K., Clark, G., Kollmann, P., Rymer, A. M., ... Bolton, S. J. (2018). Intervals of Intense Energetic Electron Beams Over Jupiter's Poles. *Journal of Geophysical Research: Space Physics*, *123*(3), 1989–1999. doi: 10.1002/2017JA025106

Szalay, J. R., Allegrini, F., Bagenal, F., Bolton, S., Clark, G., Connerney, J. E. P., ... Wilson, R. J. (2017). Plasma measurements in the Jovian polar region with Juno/JADE. *Geophysical Research Letters*, *44*(14), 7122–7130. doi: 10.1002/2017GL072837

Szalay, J. R., Allegrini, F., Bagenal, F., Bolton, S. J., Bonfond, B., Clark, G., ... Wilson, R. J. (2020). Alfvénic Acceleration Sustains Ganymede's Footprint Tail Aurora. *Geophysical Research Letters*, *47*(3), e2019GL086527. doi: 10.1029/2019GL086527

Zhang, B., Delamere, P. A., Yao, Z., Bonfond, B., Lin, D., Sorathia, K. A., ... Lyon, J. G. (2021). How Jupiter's unusual magnetospheric topology structures its aurora. *Science Advances*, *7*(15), eabd1204. doi: 10.1126/sciadv.abd1204

Zhu, B., Lindstrom, C., Jun, I., Garrett, H., Kollmann, P., Paranicas, C., ... Gladstone, G. (2021). Jupiter high-energy/high-latitude electron environment from juno's jedi and uvs science instrument background noise. *Nuclear Instruments and Methods in Physics Research Section A: Accelerators, Spectrometers, Detectors and Associated Equipment*, *1002*, 165244. Retrieved from `https://`

www.sciencedirect.com/science/article/pii/S016890022100228X doi: https://doi.org/10.1016/j.nima.2021.165244